



Scalable preparation of defect-rich free-standing TiO₂ sheets with visible-light photocatalytic activity

Hanyang Gao^a, Guoxin Hu^b, Juan Sui^a, Chao Mu^b, Wenfeng Shangguan^{b,*}, Min Kong^a, Wei Shentu^a

^a School of Mechanical Engineering, Hangzhou Dianzi University, Xia Sha Higher Education Zone, 310018 Hangzhou, Zhejiang Province, China

^b School of Mechanical and Power Engineering, Shanghai Jiao Tong University, 800 Dongchuan Road, 200240 Shanghai, China



ARTICLE INFO

Keywords:
Defect-rich
Hydrogenation
Visible-light responsible
Self-assembled sheets
Flexible substrate
Free-standing

ABSTRACT

In this research, two interesting phenomena were reported and analyzed: First, two-dimensional tiny titania nanoplates (4–5 nm lateral size, 0.4–0.5 nm thickness) with rich edge-defects were found to self-assemble into free-standing thin sheets with large lateral size in a freeze-drying process with the aid of linker; Second, when subjected to a moderate hydrogenation treatment, these self-assembled sheets could be crystallized into integral anatase sheets while the edge-defects of the building blocks were maintained on the surface or inside the body of the crystal and the flexible sheet-like shape were also maintained. Based on these observations, a method for scalable preparing free-standing defect-rich TiO₂ with a two-dimensional sheet-like morphology was proposed. The defects (oxygen vacancies) endowed the TiO₂ a grayish-black color and visible-light responsibility. By using the dispersion of these defect-rich anatase sheets, a film could be densely deposited on flexible substrates in a layered structure and showed an efficient performance in acetaldehyde decomposition under the irradiation of visible light. Since it has always been a technical challenge to prepare crystallized visible-light-driven TiO₂ films on plastic substrates with a low heat tolerance, this work may also provide a new approach to this problem.

1. Introduction

TiO₂ is the most commonly employed photocatalyst due to the characteristics of low-price, large-availability, non-toxicity, and high-efficiency. Owing to the large band gap (3.2 eV), pure TiO₂ has no visible-light activity [1,2]. To enhance the absorption of the visible light, doping strategies—including, for example, carbon doping [3,4], nitrogen doping [5,6], sulfur doping [7,8]—are usually adopted. Recently, hydrogenated TiO₂ (H-TiO₂) has been recognized as a promising visible-light-driven catalyst as the active unsaturated atoms in these defect-rich particles can not only introduce impurity states or disorders into the TiO₂ lattice, but can also be used as active sites to improve the photocatalytic performance [9–13]. However, almost all the published H-TiO₂ samples [9–11,13–18] are hydrogenated from a bulk titanium oxide material, and the generated oxygen vacancies exist only on the surface of the material, leaving the interior unaffected by hydrogenation.

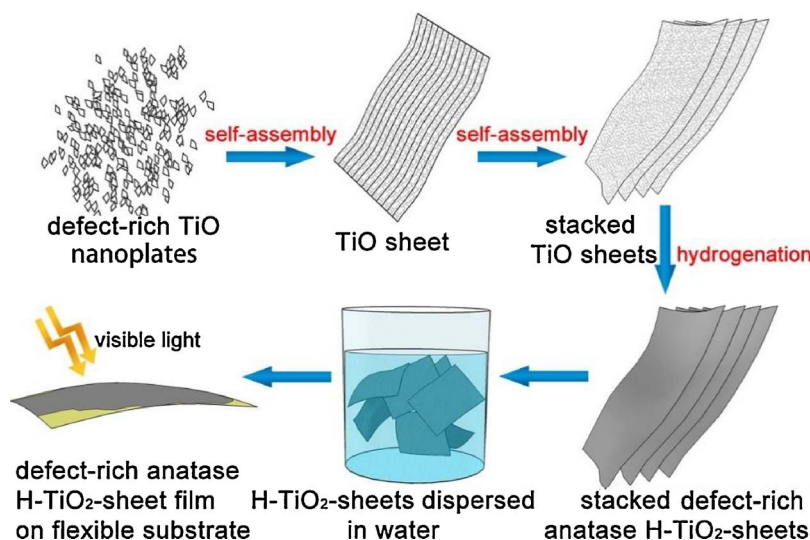
The preparation of highly crystalline TiO₂ films deposited on flexible substrates is a difficult and not completely solved problem, since the use of high-temperature annealing—which is usually a necessary step for crystallization which directly determines the catalytic

efficiency—is limited by the low heat resistance of the plastic substrates. A variety of methods has been investigated to fabricate macroscopic TiO₂ film on the plastic substrate. However, the poor crystallinity of the particles treated at a temperature lower than 150 °C weakens the connections between the particles, leading to a much lower η values of the plastic-based DSSCs—irrespective of the preparation methods—than those using glass substrates [19]. Recently, laser sinter [20] and atmospheric low-temperature roll-to-roll chemical vapor deposition method [21] was suggested to prepare the TiO₂ film on plastic substrates, but the expensive equipment and harsh conditions limited the usefulness of these methods. Because almost all the doping methods mentioned above need to be conducted at high temperatures for a long time, it is particularly challenging to prepare a visible-light-driven TiO₂ film on a flexible substrate.

In this report, free-standing anatase TiO₂ sheets with a grayish-black color and defect-rich structure were successfully synthesized by a bottom-up method from numerous tiny two-dimensional $\text{Ti}_{\square} \text{O}_{2-x}^{\delta+}$ (where \square represents oxygen vacancies, $x \approx 0.68$, named as TiO for short) nanoplates. The tiny TiO nanoplates, which possess plenty of edge-defects, were found to be able to self-assemble into a free-standing large-sized thin sheet in the freeze-drying process with the aid of a

* Corresponding author.

E-mail address: shangguan@sjtu.edu.cn (W. Shangguan).



linker. In the next hydrogenation treatment, the self-assembled sheets were crystallized into free-standing flexible anatase TiO_2 sheets with the vacancy-defects of its building blocks maintained on the surface or inside the body of the crystal. These obtained defect-rich anatase TiO_2 sheets were then dispersed in water and coated on plastic substrates to form a visible-light-driven photocatalytic film with a densely packed layered structure (Fig. 1). This method is a scalable and versatile approach to prepare free-standing, defect-rich, and sheet-like metal oxide materials. The work of preparation of MnO sheets and CoO sheets with a similar structure is in progress in our laboratory.

2. Materials and methods

2.1. Synthesis of TiO nanoplate

TiO was prepared by using a modified version of the method of Sun et al. [22]. Briefly, 0.44 g polyethylene oxide–polypropylene oxide–polyethylene oxide (Pluronic P-123, Sigma-Aldrich, USA) was dissolved in 6.67 g ethanol to make a transparent solvent (Solvent A); 2.33 g titanium isopropoxide (TTIP, Sigma-Aldrich, USA) was added into 1.64 g concentrated HCl solution (Sinopharm, China) during vigorous stirring to make Solvent B. After 30 min stirring, Solvent A was added into Solvent B and stirred for another 30 min. Then, 5.56 ml of the obtained mixture was mixed with 44.44 ml ethylene glycol (Sinopharm, China) in a round-bottomed flask equipped with a stirrer and a water-cooled reflux condenser, and heated at 120 °C for 24 h. The products were washed with ethanol for five times and water for another three times by using a washing/centrifugation method. The material was then dried at 80 °C for 24 h to obtain the TiO powder.

2.2. Synthesis of self-assembled TiO -sheet

The TiO -sheets were fabricated from the self-assembly of TiO . The TiO two-dimensional tiny particles were covalently interconnected with each other with the aid of the linker which is usually used for the connection of graphene oxide [23,24]. Typically, 5 mg/mL TiO water dispersion was mixed with 22 mM glutaraldehyde, 0.06 mM borax, and 11 mM resorcinol under rigorous stirring. After a 2 h ultrasonic treatment, the mixture was then freeze-dried in a lyophilizer for 72 h to obtain the TiO -sheet powder.

2.3. Synthesis of free-standing H- TiO_2 -sheet by hydrogenation

In the hydrogenation process, the TiO -sheet powder was annealed in H_2/Ar (1:5 v/v) flow at 400 °C for 2 h at atmospheric pressure in a

Fig. 1. Illustration of the preparation approach proposed in this study. Defect-rich self-standing anatase sheets (H- TiO_2 -sheets) were prepared from TiO nanoplates by a self-assembly and a following moderate hydrogenation treatment. These anatase sheets were loosely stacked and can be dispersed in water and deposited on a flexible substrate to make a visible-light-driven photocatalytic film.

quartz tube settled in a conventional pipe furnace (HF-Kejing, China) to obtain the grayish-black H- TiO_2 -sheet powder.

2.4. Synthesis of H- TiO_2 -sheet film on plastic substrate

To prepare H- TiO_2 -sheet film, the H- TiO -sheet powder was dispersed in water by ultrasonication for 30 min. The suspension was then coated on the substrate by using a spray coating method.

2.5. Photocatalytic decomposition of gas acetaldehyde

The photocatalytic tape with an H- TiO_2 -sheet film weighted as 100 mg as attached to the inner wall of a 125 cm³ Polyvinyl fluoride bag (Tedlar bag). After the container had been sealed, 800 ppmv gaseous acetaldehyde was injected into it. After reaching the adsorption equilibrium in dark (4 h later), the concentration of acetaldehyde was measured and used as the starting point. A 500-W xenon lamp with an intensity of 1200 W/m² was used as a light source. The UV part of the light was removed by a cutoff filter ($\lambda \geq 420$ nm) when the process was carried out under visible light irradiation. The concentrations of acetaldehyde and CO_2 were estimated by gas chromatography (GC-9200, China) respectively. In the evaluation process, 500 microliters of gas in the Tedlar bag was injected into the chromatograph with a gas tight syringe. The performance of the commercial sphere anatase TiO_2 (Aladdin, China) was recorded as a standard photocatalyst for comparison.

2.6. Material characterization

The surface morphology was examined by a JEM-2100F high resolution-transmission electron microscope (HRTEM) operated at 200 kV with a point-to-point resolution of 0.19 nm. Atomic force microscopy (AFM) measurements were carried out with an E-sweep/NanoNavi Station (SII Nanotechnology, Inc., Tokyo, Japan). Scanning tunneling microscope (SEM) was conducted on a JEOL JSM-7800F Prime system. X-ray diffraction patterns (XRD) were measured on a Rigaku D/Max-2200/PC X-ray diffractometer. X-ray photoelectron spectroscopy (XPS) detection was conducted on PHI 5000C ESCA System (Perkin Elmer Inc., USA). Raman testing was performed on a Senterra R200-L micro-Raman spectrometer (laser excitation 532 nm, Bruker Optics, Germany) at room temperature. The measurements were carried out in back-scattering configuration using an exciting wavelength of 514.5 nm from an Ar ion laser. UV-vis spectra were obtained by a SHIMADZU UV-2450 spectrophotometer. The photoluminescence (PL) performance was conducted on a LS 55 (Perkin Elmer, Inc., USA) luminescence

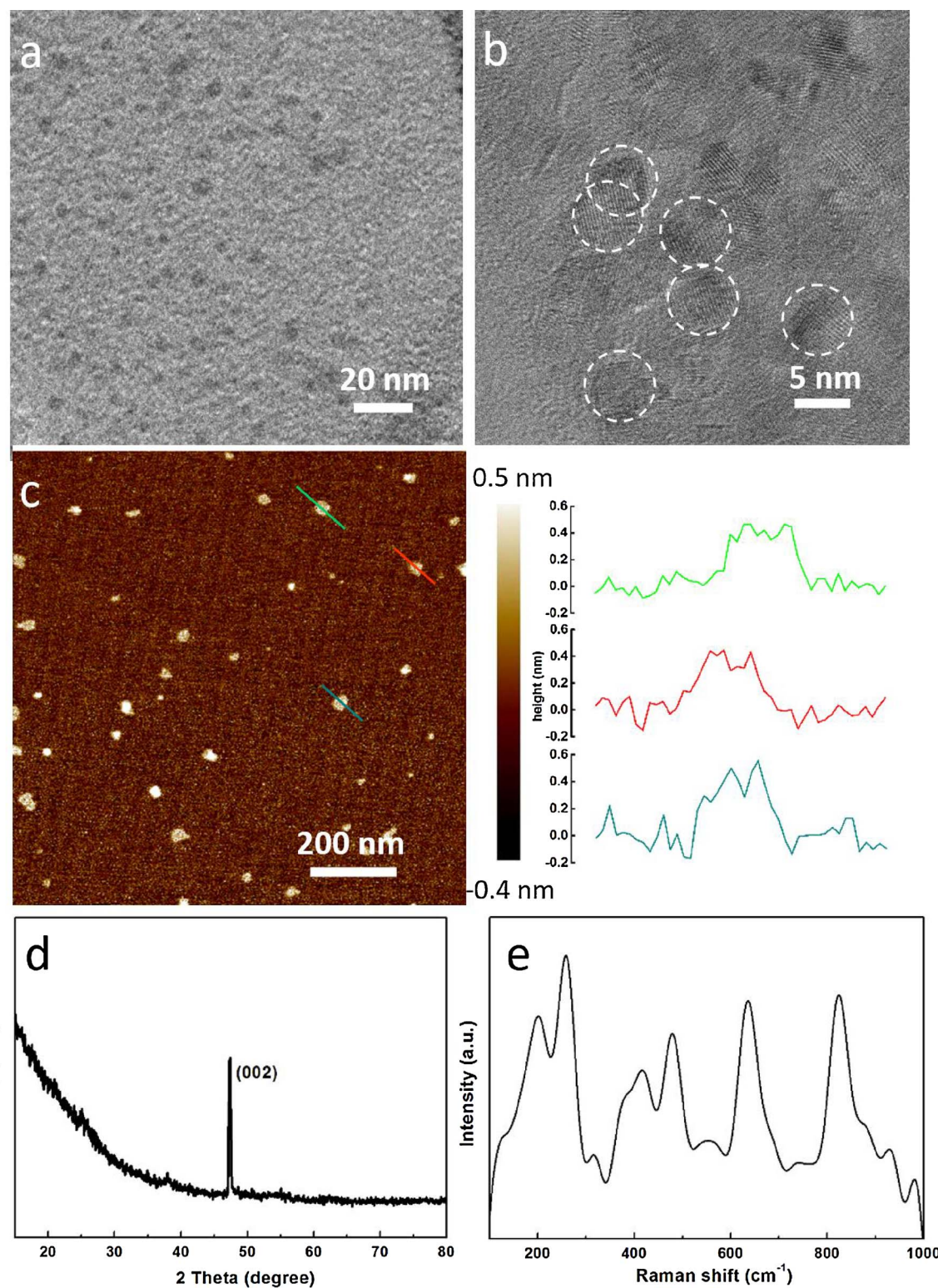


Fig. 2. The TEM image (a), HRTEM image (b), and AFM image (c) showed a flaky morphology of TiO. Only peak (002) appeared in the XRD spectrum of TiO (d). A typical octahedral structure pattern was presented in Raman spectrum (e).

spectrometer with an excitation of laser at 366 nm.

3. Results and discussion

3.1. Morphology and structure of MTQDs

The flaky morphology of TiO was visualized by AFM and TEM in

Fig. 2a–c. The lateral dimensions of typical TiO nanoplates shown in TEM image (Fig. 2a, b) were around 4–5 nm. The clear crystal lattice shown in HRTEM image (Fig. 2b) indicated that the TiO was crystallized. AFM images of TiO and the corresponding thickness profiles along the lines indicated that the thickness of TiO was extremely small—only around 0.4–0.5 nm (Fig. 2c). In the XRD spectrum, none of the characteristic peaks except peak (002) of anatase TiO₂ could be

found, indicating a unique two-dimensional single layer structure of TiO (Fig. 2d). The Raman spectrum of TiO (Fig. 2e) showed a typical pattern of the octahedral structure, indicating the nanoplate was composed of TiO₆ titanium-oxygen octahedrons [25–27].

3.2. Self-assembly behavior of TiO in freeze-drying process with the aid of linker

The forming of a well-ordered, densely packed nanosolids is a crucial step toward constructing advanced materials for technological applications and innovations [28]. It has been found in our previous studies that the tiny two-dimensional flaky TiO particulates showed a unique self-assembly behavior in the evaporation process on a wafer substrate [29,30]: Compared with sphere particles, the greater contact area endowed by their anisotropic shape between each piece, together with the plenty unsaturated dangling bonds at the periphery, made them firmly connected with each other to form a continuous film on the substrate, and left no coffee-ring after the evaporation. In this study, by exploiting self-assembly processes, a large-sized and spatially ordered nanostructure was fabricated. The linker-added TiO nanoplates tended to self-assemble into free-standing sheets with a thin thickness and a large lateral size during the freeze-drying process. The linker, which is composed of glutaraldehyde, resorcinol, and borax, has been used to fabricate aerosol-type structures from GO sheets [23,24]. It was reasonable to infer that the connections between the TiO nanoplates were enhanced by the linker. The interaction between the hydroxyl groups located on the edge of the TiO and glutaraldehyde, and the polycondensation reaction between glutaraldehyde and resorcinol [24,31], helped the TiO nanoplates to connect with each other to form a self-standing sheet.

The SEM testing recorded the self-assembly process in detail. Firstly, the TiO particulates self-assembled into long strips with length on the order of several hundred micrometers (Fig. 3a); secondly, the strips were attached to each other to construct two-dimensional sheets (Fig. 3b). These self-assembled sheets, which have a size of around several hundred micrometers or even millimeters in length and width, looked transparent and flexible under the SEM beam, suggesting a was

very thin thickness (Fig. 3b, c); next, the sheets stacked loosely into a layered structure (Fig. 3c). Fig. 3d gave the details of the self-assembly structure and its corresponding EDAX analyses indicated that the TiO nanoplates consisted of only O and Ti elements. The complete self-assembly process from TiO nanoplates the building blocks to the stacked free-standing sheets was shown in Fig. 3e.

The formation of free-standing TiO sheets is essential to the catalytic application and hard to be obtained. Compared with three-dimensional sphere TiO₂ particles, the two-dimensional self-supporting sheets 1) possess a greater surface area which can give full play to catalytic performance; 2) can be easily sprayed and deposited on a variety of substrates to form a thin film; 3) is convenient to be used and recycled. However, until the step in this section, the strength of these self-assembled sheets (connected with each other only by the electrostatic attraction), is quite low. In the next hydrogenation step, the TiO nanoplates connected together to become anatase sheets, while the flexible sheet-shaped morphology was maintained and the defects were preserved on the surface or inside the body of the anatase crystal.

3.3. The characteristics of H-TiO-sheet prepared in hydrogenation treatment

The chemical characteristics and structure of the hydrogenated derivative of TiO-sheets, the H-TiO₂-sheets, were examined in this section. A commercially available spherical anatase TiO₂ nanoparticles (sph-TiO₂ for short) with a diameter around 30 nm were also evaluated as a reference. After a hydrogenation treatment at 400 °C for 2 h, the white color of the sph-TiO₂ particles through the hydrogenation treatment was unchanged. According to the descriptions and results in previous reports, a successful hydrogenation treatment of these spherical particles is preferred to be conducted at a high-pressure condition for a long time or at a high pressure since most of the atoms are buried inside the bulk material [14–16]. Our moderate treatment condition (2 h, atmospheric pressure) was unable to meet this requirement. In contrast to the sph-TiO₂, the color of the H-TiO₂-sheet powder changed to grayish black. By a naked-eye observation, the fluffy cotton-like appearance of the powder did not seem to change much. From SEM micrograph, the two-dimensional sheet-shaped morphology and the

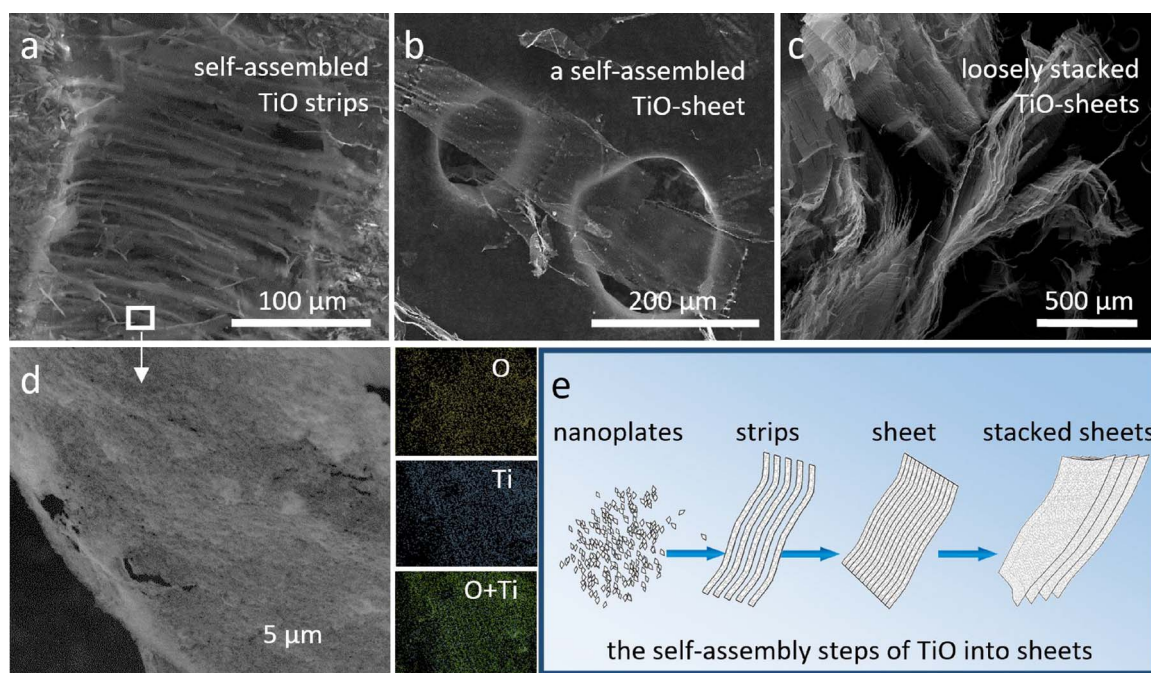


Fig. 3. The self-assembly process of TiO nanoplates into sheets during the freeze-drying process was demonstrated by SEM: (a) Firstly, the TiO nanoplates were linked together into strips; (b) second, the strips were parallelly bonded to make an ordered sheet; (c) third, the sheets were stacked with each other to form a higher-order nano-architecture. (d) The detail of the self-assembly structure and the corresponding EDAX analyses. (e) Schematic illustration showing the self-assembly steps from TiO nanoplates to stacked TiO sheets.

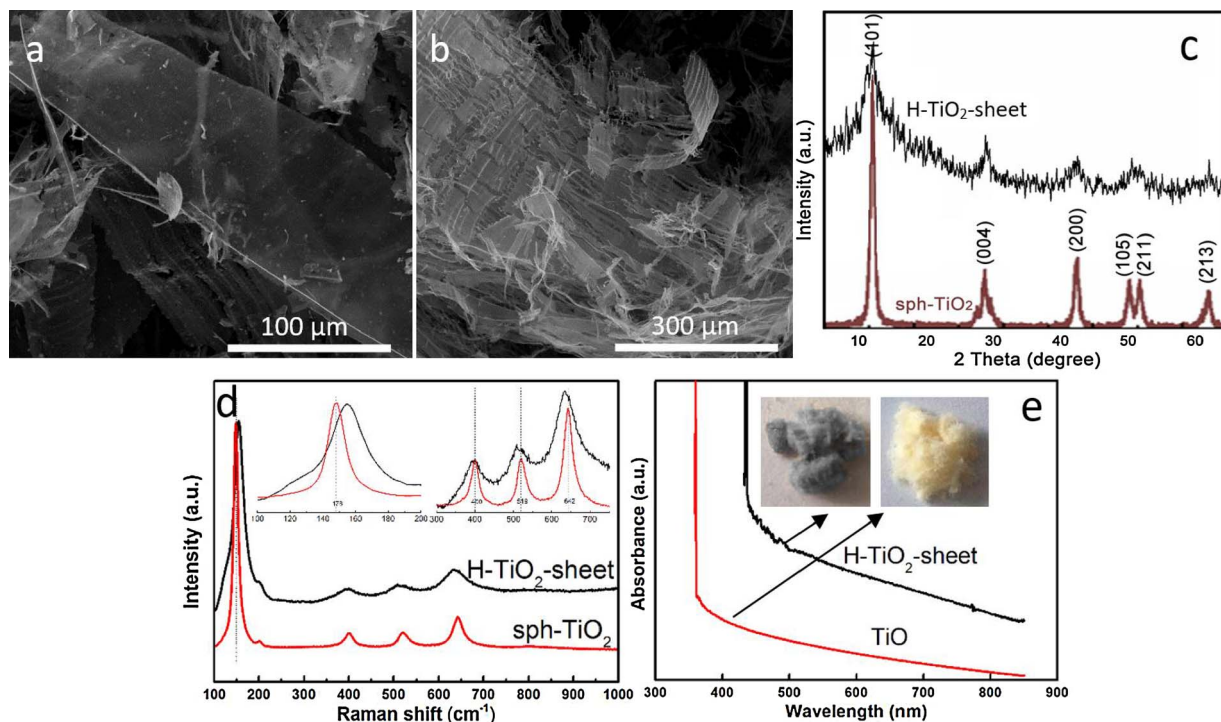


Fig. 4. (a, b) The two-dimensional sheet-like morphology was well-maintained in SEM micrograph after a moderate hydrogenation treatment. The XRD (c) and Raman (d) spectra of the H-TiO₂-sheets and sph-TiO₂ particles. (e) The optical absorbance spectrum of TiO and H-TiO₂-sheets. Inset: the photographs of TiO and H-TiO₂-sheet powder.

loosely stacked structure were found to be well preserved through the 400 °C hydrogenation (Fig. 4a, b) – the sheets did not stick together to form a three-dimensional bulk material in the hydrogen-rich environment.

Since no difference could be found in XRD, Raman, and XPS spectra between the sph-TiO₂ sample and the hydrogenated sph-TiO₂ sample, only the spectra of sph-TiO₂ were shown in the following analysis section. In XRD spectra (Fig. 4c), the emerged peaks of hydrogenated TiO (H-TiO₂-sheet) could be readily indexed to the anatase phase, indicating that the Ti and O atoms in TiO were rearranged and chemically bonded to form an anatase structure. The XRD peaks of the H-TiO₂-sheets were not as smooth as those of sph-TiO₂ particles. This should be due to the existence of plenty of defects in the crystal. Similarly, in Raman patterns (Fig. 4d), both samples showed four characteristic peaks of anatase. However, comparing with the sph-TiO₂ particles, the spectrum curve of H-TiO₂-sheet was less smooth, the 400, 519, and 642 cm⁻¹ peaks were negatively shifted, the 178 cm⁻¹ peak was positively shifted, and all the peaks were much broadened. Similar peak broadening and shift effects were recorded in previous studies about hydrogenated TiO₂ [10–12,16] and were attributed to the presence of lattice disorder originated from phonon confinement or non-stoichiometry as a result of oxygen vacancy doping [12,16,32–34]. Among all the hydrogenated samples have been reported, H-TiO₂-sheet is the most remarkable with respect both to the peak broadening degree and to the peak shifts [10–15]. Taking into account that hydrogenation condition in this study was more moderate (atmospheric pressure, short time) than those adopted in all the other references (high-pressure, longer time), it could be concluded that anatase TiO₂ sheets with plenty of oxygen-vacancy-defects could be successfully obtained under a moderate condition by using the approach proposed in our study. The depth doping of oxygen vacancy is further confirmed by the changes in UV-vis patterns shown in 4e. Different from the blue color which represents the surface oxygen vacancy, the grayish-black color reflected the existence of plenty of oxygen vacancies inside the bulk of the anatase crystal [9]. Comparing with TiO, a noticeable shift of the absorption edge into the visible light region was observed for H-TiO₂-sheet.

sheet (from 364 nm to 435 nm). The defects (oxygen vacancies) introduced disorders into the TiO₂ lattice. If the lattice disorders are plenty enough, it can produce mid-gap states which will form a continuum extending to and overlapping with the conduction band or the valence band, and narrow the band-gap of the material [15]. The apparent shift of H-TiO₂-sheet in absorption edge revealed the presence of plenty oxygen vacancies inside the bulk of the material.

More information on doping and phase transition was provided by XPS shown in Fig. 5. The Ti_{2p} and O_{1s} core levels on the surface were measured by XPS to investigate the effect of hydrogenation on the chemical oxidation and electronic state of the TiO-sheets. From XPS spectrum, no significant variation in the composition of the three samples could be observed. Comparing with TiO, the Ti_{2p3/2} peaks and Ti_{2p1/2} peaks of sph-TiO₂, and H-TiO₂-sheet moved slightly to a higher binding energy, indicating the differences in the chemical state of Ti and the formation of—considering the information provided by XRD and Raman (Fig. 4c, d)—anatase phase in H-TiO₂-sheet sample after hydrogenation treatment.

To TiO, the O_{1s} peaks are wide and asymmetric and could be fitted by four components at 530.0 eV, 530.8 eV, 532.4 eV, and 533.8 eV, ascribed to lattice oxygen of Ti–O–Ti (O_{Ti}), oxygen deficiency (O_{Def}) [35–37], surface –OH group (O_{OH}), and physisorbed H₂O (O_{H2O}) respectively (Fig. 5b). Can hardly be seen in bulk TiO₂ materials that, the percentage of lattice oxygen atoms (O_{Ti}) in TiO is quite low (only 16.6%) and 83.4% O in TiO was originated from the adsorbed species (Table 1).

$$\text{Atom}_o: \text{Atom}_{Ti} = \frac{\text{Area}_O/\text{RSF}_O}{\text{Area}_{Ti}/\text{RSF}_{Ti}} \times 100\% \quad (1)$$

The low proportion of O_{Ti} plus the appearance of O_{Def} peak which is closely related to oxygen vacancy suggested that plenty of oxygen vacancies and dangling bonds already existed in TiO (see the black dots on TiO nanoplates and TiO-sheet in Fig. 6). O_{Def} peak could be observed in the H-TiO₂-sheet sample but not in sph-TiO₂, and its percentage in TiO sample remained almost unchanged (from 8.3% to 8.9%, Table 1) after hydrogenation, indicating that the oxygen vacancies were retained after

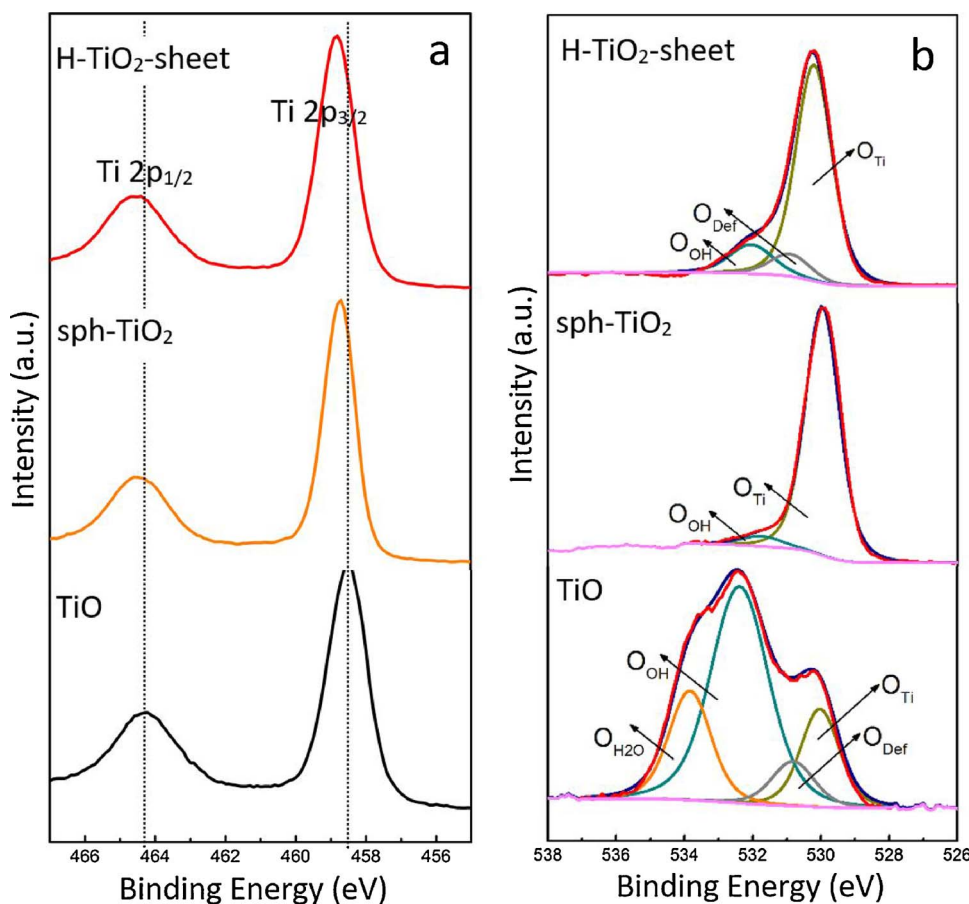


Fig. 5. The Ti_{2p} (a) and O_{1s} (b) spectra of TiO, anatase-TiO₂, and H-TiO₂-sheet. In the O_{1s} spectrum, the low proportion of O_{Ti} plus the appearance of O_{Def} peak suggested that plenty of oxygen vacancies already existed in TiO and were well-maintained in anatase H-TiO₂-sheets after the moderate hydrogenation treatment.

Table 1
Location and atom percentages of the O 1s and Ti_{2p} peaks determined by the XPS analysis.

position/percentage	TiO	H-TiO ₂ -sheet	sph-TiO ₂
O _{Ti}	530.0 eV/16.6%	530.2 eV/78.5%	529.9 eV/95.3%
O _{Def}	530.8 eV/8.3%	530.9 eV/8.9%	–
O _{OH}	532.4 eV/54.9%	532.1 eV/12.6%	531.9 eV/4.7%
O _{H2O}	533.8 eV/20.2%	–	–
O _{Ti} : Ti	1.32	2.04	2.17

Note: The atom percentages (at%) of O and Ti in each sample can be quantified by Eq. (1) [17] according to the area of the related peaks. RSF in Eq. (1) stands for relative sensitivity factor.

the hydrogenation treatment (see the black dots on H-TiO₂-sheet in Fig. 6) [17], consistent with the Raman results. The fact that the peak of O_{Ti} in H-TiO₂-sheet shifted toward a higher binding energy compared with sph-TiO₂ also indicated the presence of oxygen vacancy doping in H-TiO₂-sheet, and is well in line with other published studies reporting

the O_{1s} change of the TiO₂ samples after a hydrogenation treatment [11,13,15]. From the fact that the proportion of O_{Def} in H-TiO₂-sheet is so high and is similar with that of TiO after hydrogenation treatment, it was reasonable to deduce that these oxygen vacancies were existed not only on the surface of the H-TiO₂-sheet, but also inside the body of the material. This finding is consistent with the result in UV-vis spectrum (Fig. 7).

After hydrogenation, the adsorbed water is taken away with the gas, causing the disappearance of the O_{H2O} peak. The stoichiometric ratio of O_{Ti}/Ti increased from 1.32 to 2.03, indicating more oxygen atoms were incorporated into the lattice. This, plus the fact that the percentage of O_{OH} peak reduced from 54.9% to 12.6% with the growth of O_{Ti} percentage from 16.6% to 78.5%, and the percentage of O_{Def} remained almost unchanged, indicated that many oxygen atoms originated from the –OH had been involved in the crystallization process and changed into lattice oxygen atoms. In an H₂/Ar atmosphere of hydrogenation treatment, no oxygen atoms outside the system, but only O_{OH} could take part in the reaction. In the case of this study, O_{OH} were used as

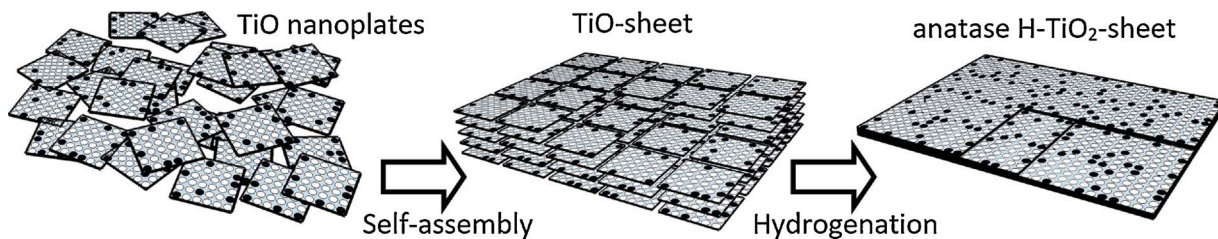


Fig. 6. Illustration of the preparation of anatase H-TiO₂-sheet from TiO nanoplates in a self-assembly and following hydrogenation process. Plenty of oxygen vacancies (black dots) have already existed on TiO, and were well maintained on the surface or inside the body of H-TiO₂-sheet after hydrogenation.

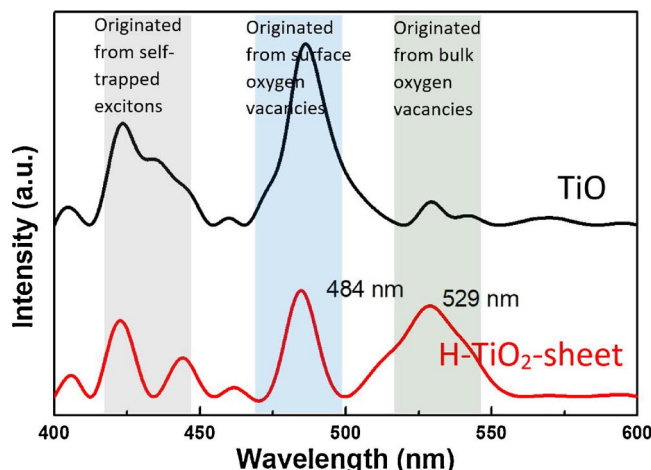


Fig. 7. PL spectrum of TiO and H-TiO₂-sheet. Since TiO is an ultrathin 2D material, the peak originated from the surface oxygen vacancies was the dominant one. For H-TiO₂-sheet, the intensity of the surface-defect-peak decreased while the internal-defect-peak was enhanced remarkably, demonstrating that a large number of defects of TiO were retained efficiently not only on the surface but also inside the body of the bulk materials during the growth of TiO into bulk materials in a hydrogen-rich environment.

used as a supply warehouse for O_{Ti}, providing a condition for the phase change into anatase.

There is another thing worth noting that, The self-assembly of TiO into a large-sized TiO-sheet with thin thickness was caused by the interaction of –OH groups—which has a close relationship with the dangling bonds—in TiO with glutaraldehyde and the polycondensation reaction between glutaraldehyde and resorcinol. According to this self-assembly behavior, it was reasonable deduced that the –OH groups mainly existed on the periphery of the TiO nanoplates.

To verify the presence of oxygen vacancies in the samples and the differences, PL emulsion spectrum—which results from the recombination of free carriers and reveals the efficiency of charge carrier trapping, migration, transfer, and separation—was performed. A comparison of PL spectra between TiO and its hydrogenated counterpart H-TiO₂-sheet was made with the excitation at 366 nm.

PL emission peaks of TiO and H-TiO₂-sheet can be divided into three main groups, which could be accordingly assigned to the emission from three physical origins: self-trapped excitons [38], oxygen vacancies (OVs) [39], and surface states [40,41]. The emission peaks in the range of 400–450 nm are attributed to the emission of self-trapped excitons located on TiO₆ [42]. The peaks at around 484 nm are originated from surface oxygen vacancies and defects of both samples [39,42], and the peaks at around 529 nm result from the oxygen vacancies buried in the bulk of materials [40,41]. For TiO, the peak originated from surface oxygen vacancies was the dominant one. In contrast, the peak resulted from the oxygen vacancies buried in bulk is not apparent. This result is consistent with the fact that, as an ultrathin 2D material, the majority of defects of TiO are exposed on the surface. For H-TiO₂-sheet, the intensity of the surface-defect-peak decreased but still maintained at a certain level. Meanwhile, the intensity of the internal-defect-peak was enhanced remarkably. This result is also in good agreement with the inference presented in the hydrogenation step in Fig. 6 that, during the growth of TiO into bulk materials in a hydrogen-rich environment, a large number of defects of TiO were retained efficiently not only on the surface but also inside the body of the bulk materials.

Consequently, it is concluded that grayish black anatase TiO₂ sheets with sizeable lateral size and very thin thickness were successfully prepared by a self-assembly and a followed hydrogenation process from

TiO. The grayish-black color was originated from a lot of oxygen vacancies—around 8.9% of the oxygen atoms—both on the surface and within the bodies of the anatase sheets. Different from a single defect in a crystal, large amounts of lattice disorder in semiconductors could yield mid-gap states which can form a band tail states merging with the valence band. These extended energy states can enhance the visible-light absorption and provide trapping sites for the photogenerated electron-hole pairs to prevent them from rapid recombination [15]. It is envisioned that these sheet materials can be easily dispersed in kinds of solvents and then be deposited on a variety of substrates to form a visible-light-absorbable film with high photocatalytic efficiency.

3.4. The H-TiO₂-sheet film deposited on flexible substrate and its photocatalytic performance

These loosely stacked H-TiO₂-sheets could be easily disassembled into dispersed isolated sheets in water by ultrasonication. Owing to the suppressed of the coffee-ring effect by the two-dimensional morphology of the particles, a densely stacked smooth anatase TiO₂ film could be conveniently prepared by a spray coating method from the dispersions on a variety of substrates at room temperature. Similar to graphene, which also possesses a two-dimensional planar structure, the H-TiO₂-sheets tended to form a film with a layer-layer structure (Fig. 8a). In this study, we sprayed the dispersion on one side of the double-sided adhesive tape to make a photocatalytic tape—which could be conveniently attached to wherever needed—the window of car or house for example—to conduct the visible-light-driven photocatalytic performance. Photocatalytic activities of samples were evaluated by photocatalytic decomposition of gas-phase acetaldehyde. The acetaldehyde decomposition rates and CO₂ evolution rates by using the H-TiO₂-sheet photocatalytic tape under the irradiation of a xenon lamp without and with a UV-cut-off-filter were shown in Fig. 8b, c. For comparison, the performance of a sph-TiO₂ film—with the same weight as the H-TiO₂-sheet—was also evaluated.

Compared with sph-TiO₂, photocatalytic activity was efficiently improved by using H-TiO₂-sheet under the irradiation of UV and visible-light (Fig. 8b). Several features of H-TiO₂-sheet may contribute to this improvement: (1) The much higher specific surface area. Benefiting from the two-dimensional sheet-like morphology, H-TiO₂-sheet possesses an enormous specific surface area of 1018 m²/g, much greater than that of the commercial sph-TiO₂ (52 m²/g). (2) The existence of plenty of defects. These intentionally created defects provide active sites for photocatalytic performance, and many reported experimental studies confirmed that the active sites play an important role in photocatalytic activity enhancement. (3) The stacked layered structure. Contrary to the regular point-to-point contact between the sphere-shaped particles, the two-dimensional sheet-like morphology and the plane-to-plane contact in the H-TiO₂-sheet film drastically increase the contact area between the particles, and improve the transfer and utilization of the photogenerated electrons. Under visible light irradiation, H-TiO₂-sheet displayed an efficient catalytic performance in acetaldehyde decomposition while sph-TiO₂ did not show any activity owing to the wide bandgap (Fig. 8c). This result is consistent with the above characterization results, also shows, and confirmed that designing defect-rich nanostructures with more active sites and a two-dimensional sheet-like morphology is a promising strategy to obtain an efficient visible-light-driven catalytic film.

4. Conclusions

In this research, a novel method to prepare defect-rich materials with a sheet-like morphology was proposed. This approach is simple

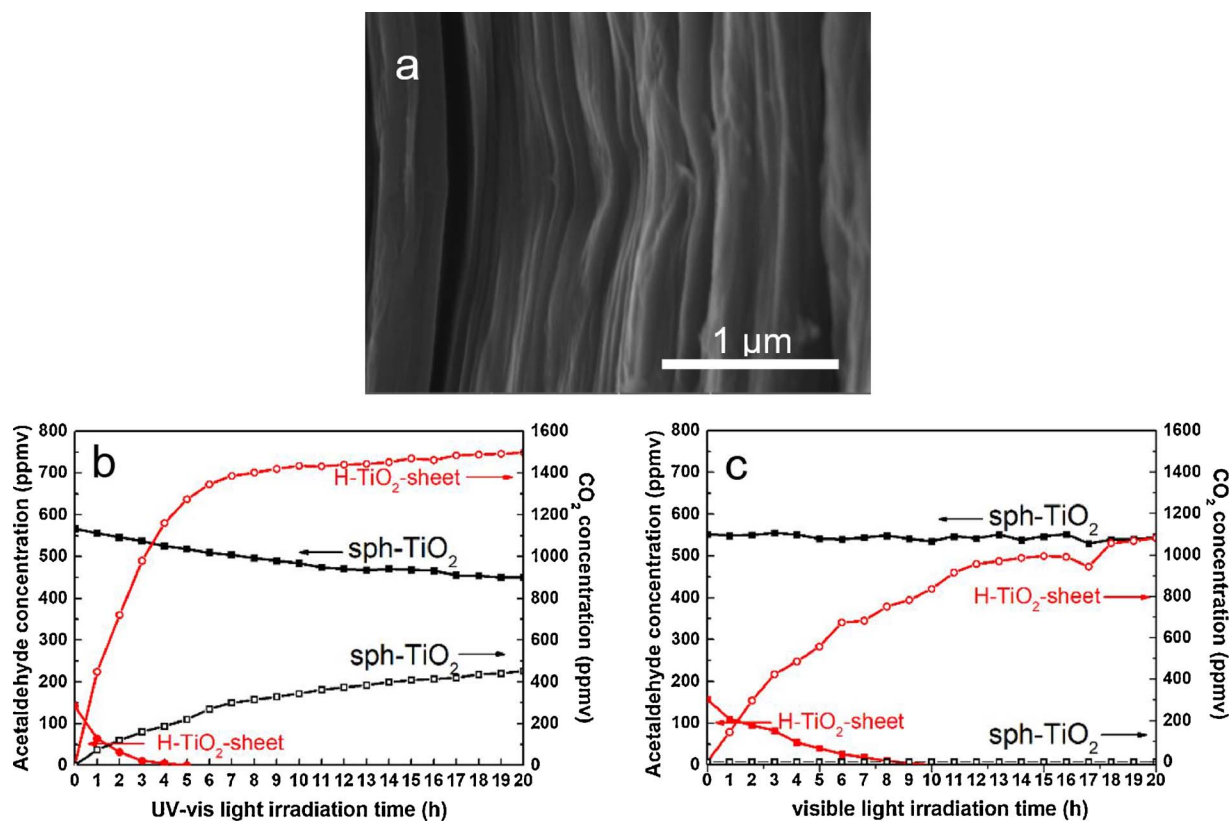


Fig. 8. (a) The layer-stacked structure of the H-TiO₂-sheet film deposited on the flexible substrate. Time courses of gas phase acetaldehyde concentration and CO₂ evolution over an H-TiO₂-sheet film and a commercial anatase sph-TiO₂ powder film under UV-vis light (b) or visible light (c). The tests used a 500 W xenon lamp and 0.1 g catalyst.

but versatile. It can be used to fabricate, for example, a visible-light responsible crystallized TiO₂ photocatalytic film with a layered structure on a flexible substrate.

In this approach, firstly, tiny two-dimensional particles with plenty of edge-defects were prepared. These nanoplates were then self-assembled into large-sized sheets with a thin thickness in freeze-drying process with the aid of a linker. Next, hydrogenation treatment at 400 °C under an atmospheric pressure was employed. In hydrogenation treatment, the thin-sheet morphology was kept, and the oxygen vacancies were also maintained on the surface or in the body of the bulk material. Due to this defect-rich characteristic, these grayish-black anatase thin sheets have visible light activity. A smooth film with layered structure was then fabricated by a simple spray coating method from these anatase thin sheets dispersions on a plastic substrate. Photocatalytic testing confirmed that the film showed an efficient photocatalytic performance on acetaldehyde decomposition under visible light. The film can be affixed to any place where is irradiated with visible light and the pollutants in air are needed to be cleaned.

Acknowledgments

We gratefully acknowledge financial support by the National Natural Science Foundation of China (51506124). We also thank the Instrumental Analysis Center of Shanghai Jiao Tong University for materials characterization.

References

- [1] G. Liu, H.G. Yang, X. Wang, L. Cheng, J. Pan, G.Q. Lu, H.-M. Cheng, Visible light responsive nitrogen doped anatase TiO₂ sheets with dominant {001} facets derived from TiN, *J. Am. Chem. Soc.* 131 (2009) 12868–12869.
- [2] R.S. Sprick, B. Bonillo, R. Clowes, P. Guiglion, N.J. Brownbill, B.J. Slater, F. Blanc, M.A. Zwijnenburg, D.J. Adams, A.I. Cooper, Visible-light-driven hydrogen evolution using planarized conjugated polymer photocatalysts, *Angew. Chem. Int. Ed.* 55 (2016) 1792–1796.
- [3] J. Liu, Q. Zhang, J. Yang, H. Ma, M.O. Tade, S. Wang, J. Liu, Facile synthesis of carbon-doped mesoporous anatase TiO₂ for the enhanced visible-light driven photocatalysis, *Chem. Commun.* 50 (2014) 13971–13974.
- [4] R. Kavitha, L.G. Devi, Synergistic effect between carbon dopant in titania lattice and surface carbonaceous species for enhancing the visible light photocatalysis, *J. Environ. Chem. Eng.* 2 (2014) 857–867.
- [5] W.-J. Ong, L.-L. Tan, S.-P. Chai, S.-T. Yong, A.R. Mohamed, Self-assembly of nitrogen-doped TiO₂ with exposed {001} facets on a graphene scaffold as photoactive hybrid nanostructures for reduction of carbon dioxide to methane, *Nano Res.* 7 (2014) 1528–1547.
- [6] C.L. Muñich, J.Y. Westcott IV, T. Fuerst, A.W. Weimer, C.B. Musgrave, Increasing the photocatalytic activity of anatase TiO₂ through B, C, and N doping, *J. Phys. Chem. C* 118 (2014) 27415–27427.
- [7] A. Eslami, M.M. Amini, A.R. Yazdanbakhsh, A. Mohseni-Bandpei, A.A. Safari, A. Asadi, N, S co-doped TiO₂ nanoparticles and nanosheets in simulated solar light for photocatalytic degradation of non-steroidal anti-inflammatory drugs in water: a comparative study, *J. Chem. Technol. Biotechnol.* 91 (2016) 2693–2704.
- [8] M.M. Momeni, Y. Ghayeb, Z. Ghonchehgi, Visible light activity of sulfur-doped TiO₂ nanostructure photoelectrodes prepared by single-step electrochemical anodizing process, *J. Solid State Electrochem.* 19 (2015) 1359–1366.
- [9] J. Qiu, S. Li, E. Gray, H. Liu, Q.-F. Gu, C. Sun, C. Lai, H. Zhao, S. Zhang, Hydrogenation synthesis of blue TiO₂ for high-performance lithium-ion batteries, *J. Phys. Chem. C* 118 (2014) 8824–8830.
- [10] X. Lu, G. Wang, T. Zhai, M. Yu, J. Gan, Y. Tong, Y. Li, Hydrogenated TiO₂ nanotube arrays for supercapacitors, *Nano Lett.* 12 (2012) 1690–1696.
- [11] T. Xia, C. Zhang, N.A. Oyler, X. Chen, Hydrogenated TiO₂ nanocrystals: a novel microwave absorbing material, *Adv. Mater.* 25 (2013) 6905–6910.
- [12] W.-D. Zhu, C.-W. Wang, J.-B. Chen, D.-S. Li, F. Zhou, H.-L. Zhang, Enhanced field emission from hydrogenated TiO₂ nanotube arrays, *Nanotechnology* 23 (2012) 455204.
- [13] N. Liu, C. Schneider, D. Freitag, M. Hartmann, U. Venkatesan, J. Müller, E. Spiecker, P. Schmuki, Black TiO₂ nanotubes: cocatalyst-free open-circuit hydrogen generation, *Nano Lett.* 14 (2014) 3309–3313.
- [14] X. Jiang, Y. Zhang, J. Jiang, Y. Rong, Y. Wang, Y. Wu, C. Pan, Characterization of oxygen vacancy associates within hydrogenated TiO₂: a positron annihilation study, *J. Phys. Chem. C* 116 (2012) 22619–22624.
- [15] X. Chen, L. Liu, Y.Y. Peter, S.S. Mao, Increasing solar absorption for photocatalysis with black hydrogenated titanium dioxide nanocrystals, *Science* 331 (2011) 746–750.
- [16] T. Leshuk, R. Parviz, P. Everett, H. Krishnakumar, R.A. Varin, F. Gu, Photocatalytic activity of hydrogenated TiO₂, *ACS Appl. Mater. Interfaces* 5 (2013) 1892–1895.
- [17] S. Li, J. Qiu, M. Ling, F. Peng, B. Wood, S. Zhang, Photoelectrochemical

- characterization of hydrogenated TiO₂ nanotubes as photoanodes for sensing applications, *ACS Appl. Mater. Interfaces* 5 (2013) 11129–11135.
- [18] T. Xia, Y. Cao, N.A. Oyler, J. Murowchick, L. Liu, X. Chen, Strong microwave absorption of hydrogenated wide bandgap semiconductor nanoparticles, *ACS Appl. Mater. Interfaces* 7 (2015) 10407–10413.
- [19] M.G. Kang, N.-G. Park, K.S. Ryu, S.H. Chang, K.-J. Kim, Flexible dye-sensitized solar cells with TiO₂ film deposited on ITO/SiO_x/metal foil substrate, meeting abstracts, *Electrochem. Soc.* (2006) 92–92.
- [20] S. Malyukov, A. Sayenko, I. Kirichenko, Laser sintering of a TiO₂ nanoporous film on a flexible substrate for application in solar cells, *Semiconductors* 9 (2016) 1198–1202.
- [21] S. Jagadeesan, Y.H. Doh, K.-H. Choi, Low-temperature fabrication of TiO₂ film on flexible substrate by atmospheric roll-to-roll CVD, *J. Coat. Technol. Res.* 3 (2017) 701–708.
- [22] Z. Sun, T. Liao, Y. Dou, S.M. Hwang, M.-S. Park, L. Jiang, J.H. Kim, S.X. Dou, Generalized self-assembly of scalable two-dimensional transition metal oxide nanosheets, *Nat. Commun.* 5 (2014) 3813.
- [23] R. Chen, J. Yan, Y. Liu, J. Li, Three-dimensional nitrogen-doped graphene/MnO nanoparticle hybrids as a high-performance catalyst for oxygen reduction reaction, *J. Phys. Chem. C* 119 (2015) 8032–8037.
- [24] P.M. Sudeep, T.N. Narayanan, A. Ganesan, M.M. Shaijumon, H. Yang, S. Ozden, P.K. Patra, M. Pasquali, R. Vajtai, S. Ganguli, Covalently interconnected three-dimensional graphene oxide solids, *ACS nano* 7 (2013) 7034–7040.
- [25] T. Gao, H. Fjellvåg, P. Norby, Raman scattering properties of a protonic titanate $\text{hxTi}_{2-x}/4\text{x}/4\text{O}_4\text{H}_2\text{O}$ (, vacancy; $x = 0.7$) with lepidocrocite-type layered structure, *J. Phys. Chem. B* 112 (2008) 9400–9405.
- [26] T. Gao, H. Fjellvåg, P. Norby, Crystal structures of titanate nanotubes: a Raman scattering study, *Inorg. Chem.* 48 (2009) 1423–1432.
- [27] T. Sasaki, S. Nakano, S. Yamauchi, M. Watanabe, Fabrication of titanium dioxide thin flakes and their porous aggregate, *Chem. Mater.* 9 (1997) 602–608.
- [28] J.J. Urban, D.V. Talapin, E.V. Shevchenko, C.B. Murray, Self-assembly of PbTe quantum dots into nanocrystal superlattices and glassy films, *J. Am. Chem. Soc.* 128 (2006) 3248–3255.
- [29] H. Gao, G. Hu, W. Shangguan, K. Zhu, Colloidal monolayer titania quantum dots prepared by hydrothermal synthesis in supercritical water, *J. Supercrit. Fluids* 88 (2014) 126–133.
- [30] H. Gao, W. Shangguan, G. Hu, K. Zhu, Preparation and photocatalytic performance of transparent titania film from monolayer titania quantum dots, *Appl. Catal. B: Environ.* 180 (2016) 416–423.
- [31] P.M. Sudeep, T.N. Narayanan, A. Ganesan, M.M. Shaijumon, H. Yang, S. Ozden, P.K. Patra, M. Pasquali, R. Vajtai, S. Ganguli, A.K. Roy, M.R. Anantharaman, P.M. Ajayan, Covalently interconnected three-dimensional graphene oxide solids, *ACS Nano* 7 (2013) 7034–7040.
- [32] A. Naldoni, M. Allietta, S. Santangelo, M. Marelli, F. Fabbri, S. Cappelli, C.L. Bianchi, R. Psaro, V. Dal Santo, Effect of nature and location of defects on bandgap narrowing in black TiO₂ nanoparticles, *J. Am. Chem. Soc.* 134 (2012) 7600–7603.
- [33] X. Chen, S.S. Mao, Titanium dioxide nanomaterials: synthesis, properties, modifications, and applications, *Chem. Rev.* 107 (2007) 2891–2959.
- [34] W. Zhang, Y. He, M. Zhang, Z. Yin, Q. Chen, Raman scattering study on anatase TiO₂ nanocrystals, *J. Phys. D: Appl. Phys.* 33 (2000) 912.
- [35] S.H. Hwang, J. Song, Y. Jung, O.Y. Kweon, H. Song, J. Jang, Electrospun ZnO/TiO₂ composite nanofibers as a bactericidal agent, *Chem. Commun.* 47 (2011) 9164–9166.
- [36] C.-T. Wang, J.-C. Lin, Surface nature of nanoparticle zinc-titanium oxide aerogel catalysts, *Appl. Surf. Sci.* 254 (2008) 4500–4507.
- [37] M. Chen, X. Wang, Y.H. Yu, Z.L. Pei, X.D. Bai, C. Sun, R.F. Huang, L.S. Wen, X-ray photoelectron spectroscopy and auger electron spectroscopy studies of Al-doped ZnO films, *Appl. Surf. Sci.* 158 (2000) 134–140.
- [38] H. Tang, H. Berger, P.E. Schmid, F. Lévy, G. Burri, Photoluminescence in TiO₂ anatase single crystals, *Solid State Commun.* 87 (1993) 847–850.
- [39] Q. Xiang, K. Lv, J. Yu, Pivotal role of fluorine in enhanced photocatalytic activity of anatase TiO₂ nanosheets with dominant (001) facets for the photocatalytic degradation of acetone in air, *Appl. Catal. B: Environ.* 96 (2010) 557–564.
- [40] Y. Lei, L.D. Zhang, G.W. Meng, G.H. Li, X.Y. Zhang, C.H. Liang, W. Chen, S.X. Wang, Preparation and photoluminescence of highly ordered TiO₂ nanowire arrays, *Appl. Phys. Lett.* 78 (2001) 1125–1127.
- [41] L.V. Saraf, S.I. Patil, S.B. Ogale, S.R. Sainkar, S.T. Kshirsager, Synthesis of nanoparticle TiO₂ by ion beam sputtering and cold condensation technique, *Int. J. Mod. Phys. B* 12 (1998) 2635–2647.
- [42] X. Li, C. Gao, J. Wang, B. Lu, W. Chen, J. Song, S. Zhang, Z. Zhang, X. Pan, E. Xie, TiO₂ films with rich bulk oxygen vacancies prepared by electrospinning for dye-sensitized solar cells, *J. Power Sources* 214 (2012) 244–250.